Journal of Operation and Automation in Power Engineering
Vol. 5, No. 1, June 2017, Pages: 83-95
http://joape.uma.ac.ir

Yaw Rate Control and Actuator Fault Detection and Isolation for a Four Wheel Independent Drive Electric Vehicle

N. Bagheri, H. Alipour *

Department of Electrical Engineering, Shabestar Branch, Islamic Azad University, Shabestar, Iran.

Abstract- *In this paper, a new actuator fault detection and isolation method for a four wheel independent drive electric vehicle is proposed. Also, a controller based on sliding mode control method is proposed for lateral stability of the vehicle. The proposed control method is designed in three high, medium and low levels. At the high-level, the vehicle desired dynamics such as longitudinal speed reference and yaw rate reference are determined. The medium-level is designed to achieve desired traction force and yaw moment based on the sliding mode control. At the low-level, by defining and optimally minimizing a cost function, proper force or torque signals are determined to apply to the wheels. Moreover, this paper also presents a new method for actuator fault detection and isolation in electric vehicles. The proposed fault detection method uses comparison of sliding ratio of different wheels. Using the proposed method, value of the actuator fault and its position are accurately estimated and diagnosed. Then, the proposed controller is modified and adapted to new conditions using the fault identification results. Finally, the validity of proposed controller is confirmed by the conducted simulations in MATLAB and CARSIM environments.*

Keyword: Fault detection, Four wheel drive electric vehicle, Sliding mode control, Vehicle lateral stability.

NOMENCLATURE

a_x ,a_y	Vehicle longitudinal and lateral acceleration
a_{rx}	Requested vehicle longitudinal acceleration
A	Vehicle front area
C_D	Aerodynamic drag coefficient
C_f , C_r	Stiffness coefficients of front and rear wheels
F_{xi}, F_{yi}	Longitudinal and lateral forces of the ith wheel
F_{zi}	Normal force of the ith wheel
F_{zav}	Average normal force of the wheels
F_{zh}	Normal force of the intact wheel
F_{zf}	Normal force of the faulty wheel
h_{CG}	Height of gravity center
I_z	Yaw inertia of the vehicle
I	Wheel moment of inertia
k_i	Electric drive system gain
k_h	Gain of the intact motor
k_f	Gain of the faulty motor
m	Vehicle sprung mass
m_w	Total mass of the wheel
M	Vehicle total mass
M_z	Vehicle direct yaw moment
R_{eff}	Tire effective rolling radius
s_i	Tire longitudinal slip ratio of the ith wheel
T_i	Output torque of the motor
u_i	Control input to the ith motor driver
u_h	Control signal of the intact motor
u_f	Control signal of the faulty motor
V_x	Vehicle longitudinal speed at mass center
V_y	Vehicle lateral speed at mass center
V_{xref}	Reference longitudinal speed
ω_i	Angular velocity of the i-th wheel
ρ_a	Air density
δ	Wheel steering angle
β	Vehicle body sideslip angle
μ	Adhesive coefficient between tire and road
θ_{vi}	Lateral tire slip angle
γ	Vehicle yaw rate
γ_{ref}	Yaw rate reference
ζ_i	Linearized curve slope

Received: 17 Apr. 2016
Revised: 01 Oct. 2016
Accepted: 20 Nov. 2016
∗Corresponding author:
E-mail: hasan.alipour2006@gmail.com (H.Alipour)

1. INTRODUCTION

Four-wheel independent drive electric vehicle (4WID-EV) with in-wheel motors is a new structure for electric vehicles. These vehicles use four in-wheel motors with

the possibility of independent torque control [1]. In-wheel motor provides greater flexibility to the vehicle's integration through removing central traction motor and mechanical differential.

Some new problems such as vehicle stability, EV battery charging, and electric retail market issues are growing with EVs developments [2]. The main problem of 4WID-EV is the need a control system to guarantee the vehicle stability at turns, especially when a fault occurs in one of the traction motors [3-5]. Therefore, a 4WID-EV needs an appropriate actuator torque control system to have a safe trip, especially when an actuator fault is occurred. in addition, due to the fact that these vehicles are more vulnerable to the faults in electric motors than vehicles with differential, therefore a fault identification system and a controller adaptation system to new conditions are extremely required. Thus, providing new fault tolerant controllers and fault detection and isolating systems for 4WID-EVs are interesting research topics to automobile industry researchers.

A fuzzy yaw rate controller for a 4WID-EV with independent control of each wheel slip rate along with a reference yaw rate generation by using neural network have been presented in [6-9]. In [10], a three-layer control has been proposed to guarantee the vehicle stability of a 4WID-EV with DC in-wheel motors. In [10], using fuzzy logic controller, the optimum amount of wheels slip is determined first and then the sliding mode controller is used to drive DC motors. In [11], a yaw moment controller has been proposed for vehicle stability control. In this reference, the optimal yaw moment is obtained by minimizing a cost function. This cost function is defined by using error of yaw rate from its reference and the body lateral slip angle. [12] uses a fuzzy logic controller for controlling the motor and hydroelectric brakes to ensure the lateral stability of the vehicle. The assumed vehicle in this reference is a hybrid electric vehicle, which can be charged through the Road (TTR) with a gasoline engine on the front axle and an electric motor on the rear axle.

In [13], a proportional and integral sliding mode controller is proposed for 4WID vehicles and [14] proposes a method for controlling the vehicle on slippery roads. A combined fault-tolerant controller with the use of linear square control method and Lyapunov function technique is presented in [15]. [16] suggested an adaptive passive fault-tolerant controller. To design this controller, the vehicle is modeled with three degrees of freedom and Lyapunov function technique is used. In [17], the fault-tolerant controller using sliding mode control has been proposed for multi-acuator systems such as 4WID vehicles. [18] attempts to identify and isolate faults in electric actuators of 4WID-EVs using an estimate of road-tire adhesion coefficient. However, the proposed method is effective when the output torque of the four motors are equal, so it would not respond in conditions such as turns where the motors experience different torques. In [19] and [20], to control low speed vehicles such as vehicles used for load and containers displacement, physical relationships of DC motors and wheel mechanics as well as band model graph have been used; though, the proposed method does not estimate the value of fault. [21] presents a model based method for the fault detection and isolation in electric drive using machine learning technologies. However, this method is used only for identifying several known malfunctions, which are defined in the detection algorithms database. An Electric differential (ED) has been presented in [22].

This ED is the developed version of the proposed ED in [23] for 4WID-EVs. In [22], the synchronization action is achieved by using a fictitious Master technique, and the Ackerman principle is used to compute an adaptive desired wheel speed. Although, the performance of this ED can be acceptable in normal driving conditions, vehicle stability is not guaranteed in critical conditions such as driving on slippery roads, severe steering angle changes, and in case of an unskilled driver. An optimal torque distribution control strategy for 4WID-EVs is proposed in [24].

In [24], at first, using a PID controller and relations between the vehicle parameters, the desired CG longitudinal force, lateral force and yaw moment are defined. Then, a cost function is defined to minimize the difference between the vehicle longitudinal force, lateral force and yaw moment with their desired values. The cost function is optimally minimized with considering tire-road adhesion. Consequently, vehicle can be stable on the slippery roads.

However, robustness is not considered. [25] proposes a direct yaw moment control with the electric motor-based and the friction brake-based actuation of the stability control for two motors drive vehicle. However, this approach cannot be applied to 4WID-EV, directly. [26] presents a SMC and a proportional-integral SMC (PISMC) to control the longitudinal velocity, lateral velocity, and yaw rate of a 4WID-EV. This controller is a passive fault tolerant controller without any fault detection or isolation properties. It can have suitable performance in normal driving conditions.

Although, the vehicle may be unstable on the slippery loads. [27] presents an electronic stability control

algorithm for the 4WID-EV. A stability judgment controller, an upper level controller, and a torque distribution strategy are designed using PID and fuzzy logic controllers. This method provides a suitable tracking of the trajectory, the side slip angle and the yaw rate at high speed on roads with a low adhesion coefficient. However, the faulty condition has not been considered.

In the present paper, a new yaw rate controller for 4WID-EVs is presented. Furthermore, a novel actuator faut detection and isolation method is proposed and the designed controller is adapted for the new condition based on fault identification results. Based on authors' knowledge, the proposed method is new and it is not proposed in the previoused published literatures.

For the remain of the paper, the vehicle and tire model is presented in Section 2. Sections 3 and 4 explain the proposed control structure and fault detection and isolation method, respectively. Simulation results are presented in Section 5; and finally, Concluding remarks are stated in Section 6.

2. SYSTEM MODELING

2.1. Vehicle Model

Ignoring the pitch and roll motions, the vehicle has three degrees of freedom to move in a longitudinal, lateral and rotational (yaw) form in a horizontal plane. Fig. 1 indicates a simplified schematic of a vehicle model in the horizontal plane [16].

In Figure 1, CG represents the gravity center of the vehicle. Vehicle dynamics equations can be stated as Eq. (1) [16].

$$\begin{cases} M\dot{V}_x = (F_{xfl}+F_{xfr})\cos\delta - (F_{yfl}+F_{yfr})\sin\delta \\ \quad + F_{xrl}+F_{xrr} - \frac{1}{2}\rho_a C_D A V_x^2 + MV_y\gamma \\ M\dot{V}_y = (F_{yfl}+F_{yfr})\cos\delta + (F_{xfl}+F_{xfr})\sin\delta \\ \quad + F_{yrl}+F_{yrr} - MV_x\gamma \\ I_z\dot{\gamma} = (F_{yfl}\sin\delta - F_{xfl}\cos\delta + F_{xfr}\cos\delta - F_{yfr}\sin\delta)l_s \\ \quad + (F_{xrr}-F_{xrl})l_s - (F_{yfr}+F_{yrr})l_r + ((F_{xfr}+F_{xfl})\cos\delta \\ \quad + (F_{xfr}+F_{xfl})\sin\delta)l_f \end{cases} \quad (1)$$

Where, V_x and V_y, are longitudinal and lateral speed, respectively, and γ is the vehicle yaw rate. F_{xi} (i = *fl*, *fr*, *rl*, *rr*) are longitudinal forces of wheels; F_{yi} is lateral forces exerted on wheels; M the mass of the vehicle; ρ_a is air density; C_D represents air drag coefficient; A is the vehicle front area; δ is the steering wheel angle; and the distances of l_f, l_r, and l_s are also indicated in Fig. 1.

According to Eq. (1), vehicle's state-space equations can be written as follows:

$$\begin{bmatrix} \dot{V}_x \\ \dot{V}_y \\ \dot{\gamma} \end{bmatrix} = \begin{bmatrix} V_y\gamma - \frac{\rho_a C_D}{2M} A V_x^2 \\ -V_x\gamma \\ 0 \end{bmatrix} + B_y \begin{bmatrix} F_{yfl} \\ F_{yfr} \\ F_{yrl} \\ F_{yrr} \end{bmatrix} + B_x \begin{bmatrix} F_{xfl} \\ F_{xfr} \\ F_{xrl} \\ F_{xrr} \end{bmatrix} \quad (2)$$

Where, in (2), $\mathbf{B_x}$ and $\mathbf{B_y}$ are:

$$\mathbf{B_x} = \begin{bmatrix} \frac{\cos\delta}{M} & \frac{\cos\delta}{M} & \frac{1}{M} & \frac{1}{M} \\ \frac{\sin\delta}{M} & \frac{\sin\delta}{M} & 0 & 0 \\ \frac{l_f\sin\delta - l_s\cos\delta}{I_z} & \frac{l_f\sin\delta + l_s\cos\delta}{I_z} & \frac{-l_s}{I_z} & \frac{l_s}{I_z} \end{bmatrix} \quad (3)$$

$$\mathbf{B_y} = \begin{bmatrix} \frac{-\sin\delta}{M} & \frac{-\sin\delta}{M} & 0 & 0 \\ \frac{\cos\delta}{M} & \frac{\cos\delta}{M} & \frac{1}{M} & \frac{1}{M} \\ \frac{l_f\cos\delta + l_s\sin\delta}{I_z} & \frac{l_f\cos\delta - l_s\sin\delta}{I_z} & \frac{-l_r}{I_z} & \frac{l_r}{I_z} \end{bmatrix} \quad (4)$$

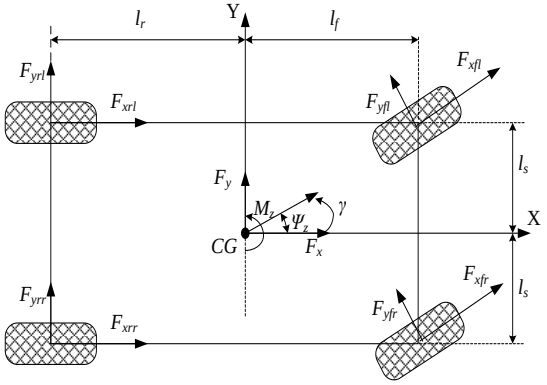

Fig. 1. Vehicle model with three degrees of freedom in horizontal plane [16]

2.2. Tire model and signals calculation

In this section, the tire model and basic wheel and tire parameters such as longitudinal and lateral wheel slip, movement of wheels normal force (load transfer) during braking, acceleration and cornering as well as longitudinal and lateral forces between the tire and the road are modeled.

2.2.1. Wheel slip

There are two types of wheel slip including longitudinal and lateral wheel slip. Due to the natural flexibility of the tire, it is observed that the distance traveled by a tire is different from its expected peripheral speed. To express this phenomenon, the term "longitudinal slip" is used. Equation Eq. (5) indicates the longitudinal *i*-th wheel slip ratio.

In this equation, Reff is the effective wheel radius; ωi is the i-th wheel angular velocity and Vxi is the longitudinal velocity of wheel center.

$$s_i = \frac{\omega_i R_{eff} - V_{xi}}{\max(V_{xi}, \omega_i R_{eff})} \tag{5}$$

The longitudinal speed of wheels' center is calculated by Eq. (6) [16].

$$\begin{cases} V_{Xfl} = (V_x - \gamma l_s)\cos\delta + (V_y + \gamma l_f)\sin\delta \\ V_{Xfr} = (V_x + \gamma l_s)\cos\delta + (V_y + \gamma l_f)\sin\delta \\ V_{Xrl} = V_x - \gamma l_s \\ V_{Xrr} = V_x + \gamma l_s \end{cases} \tag{6}$$

The ratio of lateral wheel speed to its longitudinal speed is called lateral slip. It is represented by θ_{vf} for front wheels and by θ_{vr} for the rear wheels.

In case these angles are small, we can calculate the tire lateral forces as follows [28]:

$$\begin{cases} F_{yfr} \cong F_{yfl} \cong C_f(\delta - \theta_{vf}) \\ F_{yrr} \cong F_{yrr} \cong C_r(-\theta_{vr}) \\ \tan(\theta_{vf}) = \beta + \dfrac{l_f \gamma}{V_x} \\ \tan(\theta_{vr}) = \beta - \dfrac{l_r \gamma}{V_x} \end{cases} \tag{7}$$

$$with \quad \beta = \tan^{-1}\left(\frac{V_y}{V_x}\right)$$

In the above equation, β is the vehicle body sideslip angle, and C_f and C_r are stiffness coefficients of front and rear wheels, receptively.

2.2.2. Load transfer model

Suspension system and sprung mass in vehicle cause load displacement during vehicle's acceleration, braking and cornering movement. In other words, the vertical force applied on the wheels' center changes. It is worth to note that the maximum applicable force to each wheel in order to guarantee its stable operation, depends on the wheel normal force. If F_{zi} is the *i*th wheel normal force and μ is the adhesive coefficient between tire and road, the maximum force that can be applied on each wheel to maintain the vehicle stability equals:

$$F_{\max i} = \mu . F_{zi} \tag{8}$$

The wheels' normal forces can be calculated in the form of Eq. (9) [16]. In this regard, h_{CG} is the height of gravity center and m_w is the total mass of the wheel.

$$\begin{aligned} F_{zfl} &= m_w g + \frac{mgl_r}{2(l_r + l_f)} - \frac{mh_{CG}a_x}{2(l_r + l_f)} - \frac{mh_{CG}a_y}{4l_s} \\ F_{zfr} &= m_w g + \frac{mgl_r}{2(l_r + l_f)} - \frac{mh_{CG}a_x}{2(l_r + l_f)} + \frac{mh_{CG}a_y}{4l_s} \end{aligned} \tag{9}$$

$$\begin{aligned} F_{zrl} &= m_w g + \frac{mgl_f}{2(l_r + l_f)} + \frac{mh_{CG}a_x}{2(l_r + l_f)} - \frac{mh_{CG}a_y}{4l_s} \\ F_{zrr} &= m_w g + \frac{mgl_f}{2(l_r + l_f)} + \frac{mh_{CG}a_x}{2(l_r + l_f)} + \frac{mh_{CG}a_y}{4l_s} \end{aligned}$$

2.2.3. Magic tire formula

Tires longitudinal force (F_{xi}) and lateral force (F_{yi}) have non-linear functions of the longitudinal slip ratio (s_i) and the lateral tire slip angle (θ_{vi}). This non-linear equation is as Eq. (10) and called magic tire formula [14].

$$\begin{aligned} &y(x) = D\sin\left[C\tan^{-1}(Bx - E(Bx - \tan^{-1}(Bx)))\right] \\ &Y(X) = y(x) + S_v \\ &x = X + S_h \end{aligned} \tag{10}$$

The outputs of the above equation (y (x)) are F_{xi} and F_{yi} and the input signal (x) can be s_i or θ_{vi}. In Eq. (10), coefficients *B*, *C*, *D*, and *E* are constant coefficients depending on tire shape and material and S_v and S_h are $y(x)$ curve displacement with respect to the origin. These parameters and coefficients are set using tire experimental data [14]. To settle equation Eq. (10) with experimental results, intelligent methods such as genetic algorithms can be used [29].

According to what earlier expressed, system state equations can be stated considering β and γ as the state variables in Eq. (11) [28], where Mz is the direct yaw moment of vehicle.

$$\begin{aligned} \begin{bmatrix} \dot{\beta} \\ \dot{\gamma} \end{bmatrix} &= \begin{bmatrix} \dfrac{-2(C_f + C_r)}{MV_x} & \dfrac{2(-l_f C_f + l_r C_r)}{MV_x^2} - 1 \\ \dfrac{2(-l_f C_f + l_r C_r)}{I_z} & \dfrac{-2(l_f^2 C_f + l_r^2 C_r)}{I_z V_x} \end{bmatrix} \begin{bmatrix} \beta \\ \gamma \end{bmatrix} \\ &+ \begin{bmatrix} \dfrac{2C_f}{MV_x} \\ \dfrac{2l_f C_f}{I_z} \end{bmatrix} \delta + \begin{bmatrix} 0 \\ \dfrac{1}{I_z} \end{bmatrix} M_z \end{aligned} \tag{11}$$

3. CONTROLLING THE 4WID-EV

The proposed controller consists of three parts, namely, high-level, medium-level - and low-level controllers. The high-level controller has been designed to determine vehicle's desired dynamics including longitudinal speed and desired yaw rate. The desired amounts of these dynamics are calculated based on driver requests, signals obtained from sensors and road conditions. The medium-level controller calculates the amount of total traction force and the desired yaw moment using sliding mode controller in order to achieve the desired dynamics. Finally, low-level controller determines the necessary torques to the wheels. For this purpose, a cost function is defined based on the vehicle dynamics and is optimally minimized.

3.1. High-level controller

In controller designing for 4WID-EV, the purpose is to maintain the vehicle stable besides preparing the driver demands. Signals obtained from accelerator and brake pedals and steering wheel angle may indicate driver's demands. Therefore, reference longitudinal speed (V_{xref}) can be calculated using longitudinal acceleration request signal (brake and accelerator pedal position) (a_{rx}).

$$V_{xref} = V_{x0} + \int_{t0}^{t} a_{rx} dt \tag{12}$$

In the above equation, V_{x0} is the speed of vehicle at the time t_0.

Another important signal is the yaw rate reference (γ_{ref}), which is calculated according to steering wheel angle (δ_{sw}) and the longitudinal speed of the vehicle according to the following equation [16].

$$\gamma_{ref} = \begin{cases} \gamma_t & if\ (|\gamma_t| < \dfrac{\mu.g}{V_x}) \\ \dfrac{\mu.g}{V_x} sign(\gamma_t) & elsewhere \\ with\ \ \gamma_t = \dfrac{GR.k_a.V_x}{l.(k_b V_x^2 + 1)(\tau_1 s + 1)(\tau_2 s + 1)} \delta_{sw} \end{cases} \tag{13}$$

The parameters used in Eq. (13) and their values are introduced in Table 1.

3.2. Medium-level controller

The medium-level controllers have been designed to obtain the desired amount of traction force (F_{xdes}) and moment of appropriate yaw moment (M_{zdes}) in order to follow the desired dynamics. This level consists of two parts, the speed controller and the yaw rate controller, where the present paper used the sliding mode control method for designing.

In the sliding mode control method for a system with the state space $\dot{X}=f(X)+Bu$, with assuming an integral sliding surface according to Eq. (14), the control signal is recommended as Eq. (15) [30].

In Eq. (14), e represents error signal from the reference value; λ is a constant coefficient; and in Eq. (15), $\hat{f}(X)$ is the estimated value and k is the coefficient of the sign function. In Eq. (15), the tangent function can be used to reduce the amount of chattering over the final value instead of the sign function [31].

$$\begin{cases} S = e + \lambda \int e dt \\ e = X - X_{ref} \end{cases} \tag{14}$$

$$u = -B^{-1}(\hat{f}(X) - \dot{X}_{ref} + k_p e + k_i \int e dt + k\,\mathrm{sgn}(S)) \tag{15}$$

Table 1. Parameters for reference yaw rate calculation

	Notation	Unit	Numerical value
Time constants	τ_2 and τ_1	s	0.03601 and 0.03601
Vehicle wheel base	l	m	2.58
Adhesive coefficient between road and tire	μ	-	0.85
Gear ratio of the steering mechanical linkage	GR	-	16
Gain of the reference model	k_a	-	2.685×10^{-2}
Stability factor	k_b	-	1.788×10^{-2}

3.2.1. Designing speed controller

In order to design the speed controller, the error signal has been considered as the vehicle longitudinal speed difference with the longitudinal speed reference and the sliding surface is selected as an integral.

$$\begin{cases} S = e_v + \lambda_v \int e_v dt \\ e_v = V_x - V_{xref} \end{cases} \tag{16}$$

According to Eq. (1) and Eq. (15), the desired total traction force will be equal to Eq. (17).

$$F_{xdes} = -MV_y\gamma + M\dot{V}_{xref} + \frac{\rho_a C_D A V_x^2}{2} - M\lambda_v e_v - Mk_v \tan(S) \tag{17}$$

3.2.2. Designing yaw moment controller

The error signal is now considered as yaw rate difference from the reference value.

$$\begin{cases} S = e_\gamma + \lambda_\gamma \int e_\gamma dt \\ e_\gamma = \gamma - \gamma_{ref} \end{cases} \tag{18}$$

According to equations Eqs. (11) and (15), the desired yaw moment is calculated as follows:

$$\begin{aligned} M_{zdes} = {} & 2(l_f C_f - l_r C_r)\beta + \frac{2}{V_x}(l_f^2 C_f + l_r^2 C_r)\gamma \\ & - 2l_f C_f \delta + I_z \dot{\gamma}_{ref} - I_z \lambda_\gamma e_\gamma - I_z k_\gamma \tan(S) \end{aligned} \tag{19}$$

3.3. Low-level controller

The low-level controller is designed to obtain the amount of forces or torques applied on the wheels in order to achieve the desired values of the medium-level controller. For simplicity purposes, it is assumed that the wheels on one side of the vehicle have the similar effect on vehicle performance [16, 17]. Therefore, the force can be divided between the wheels on one side of the vehicle in accordance with the wheels normal forces. So we have:

$$\begin{cases} F_{xrl} = D_1 F_{xfl} = \dfrac{F_{zrl}}{F_{zfl}} F_{xfl} \\ F_{xrr} = D_2 F_{xfr} = \dfrac{F_{zrr}}{F_{zfr}} F_{xfr} \end{cases} \tag{20}$$

According to vehicle's low dynamics in comparison to fast dynamics of the driving in-wheel motors, the electric motors dynamics were ignored and in-wheel motors were modeled in terms of the constant gains in accordance with Eq. (21). In this equation, T_i is the output torque of the motor, u_i is the motor control signal, and k_i is the electric drive system gain.

$$k_i = \frac{T_i}{u_i} \tag{21}$$

Regarding system dynamics, the cost function is defined as Eq. (22). In this regard, ω_1 and ω_2 are weights coefficients and T_{max} is the maximum torque produced by in-wheel motor.

$$\begin{aligned} J = \omega_1 & \left[\frac{k_i u_{xfl}}{R_{eff}} (\cos\delta + D_1) + \frac{k_i u_{xfr}}{R_{eff}} (\cos\delta + D_2) - F_{xdes} \right]^2 + \\ & \omega_2 [\frac{k_i u_{xfl}}{R_{eff}} (-l_s \cos\delta - D_1 l_s + l_f \sin\delta) + \\ & \frac{k_i u_{xfr}}{R_{eff}} (l_s \cos\delta + D_2 l_s + l_f \sin\delta) - M_{zdes}]^2 \end{aligned} \tag{22}$$

$$with \quad \begin{cases} \dfrac{k_i u_{xi}}{R_{eff}} - \mu F_{zi} \le 0 \\ k_i u_{xi\,xi} - T_{\max i} \le 0 \\ i = fl, fr \end{cases}$$

By solving this cost function for normal driving conditions, the forces required to apply on wheels by in-wheel motors are obtained through solving Eq. (23).

$$\begin{cases} I. \ \dfrac{k_{fl} u_{xfl}}{R_{eff}} [\omega_1 (\cos\delta + D_1)(\cos\delta + D_2) \\ + \omega_2 (l_s \cos\delta + D_2 l_s + l_f \sin\delta)(-l_s \cos\delta - D_1 l_s + l_f \sin\delta)] \\ + \dfrac{k_{fr} u_{xfr}}{R_{eff}} [\omega_1 (\cos\delta + D_2)^2 + \omega_2 (l_s \cos\delta + D_2 l_s + l_f \sin\delta)^2] \\ = [\omega_1 (\cos\delta + D_2) F_{xdes} + \omega_2 (l_s \cos\delta + D_2 l_s + l_f \sin\delta) M_{zdes}] \\ II. \ \dfrac{k_{fl} u_{xfl}}{R_{eff}} [\omega_1 (\cos\delta + D_1)^2 + \omega_2 (-l_s \cos\delta - D_1 l_s + l_f \sin\delta)^2] \\ + \dfrac{k_{fr} u_{xfr}}{R_{eff}} [\omega_1 (\cos\delta + D_1)(\cos\delta + D_2) + \\ \omega_2 (-l_s \cos\delta - D_1 l_s + l_f \sin\delta)(l_s \cos\delta + D_2 l_s + l_f \sin\delta)] = \\ [\omega_1 (\cos\delta + D_1) F_{xdes} + \omega_2 (-l_s \cos\delta - D_1 l_s + l_f \sin\delta) M_{zdes}] \end{cases} \tag{23}$$

4. FAULT IDENTIFICATION AND CONTROLLER MODIFUCATION

Stability of four wheel drive electric vehicles heavily depends on the proper operation of in-wheel motors. However, with increasing the number of actuators, possibility of fault in vehicles' electric actuators increases and may jeopardize the stability of the vehicle and the occupant's safety. Therefore, if a fault occurs in one of the electric traction motors, the fault and its location should be detected and its value should be estimated and the controller must be modified.

4.1. Fault identification and isolation

In order to detect the fault, a new method is proposed in this paper, which can detect fault location in four wheel drive electric vehicles in various situations. Although, most malfunctions occur for in-wheel motors are bearing faults and the motor is usually producing less torque than the requested amount [16], in this article, the malfunctions are considered in two forms of reduction in in-wheel motor control gain and increase of this gain. To identify fault type, it is required to save the control signals at a moment of previous samplings and compare to current moment. At fault type identification, if the current control signal related to the faulty motor is greater than control signal at a few moments before, the gain reduction fault occurs; otherwise, there is the gain increasing malfunction. As seen in Fig. 2, the tire longitudinal force curve shows a non-linear behavior based on the longitudinal slip. The curve is divided into two stable and unstable regions [32]. The tire slips on the unstable region (slips greater than 1.1 for the given tire) and the vehicle becomes unstable. Thus, by limiting the applied force to the wheel, the tire slip must be maintained in the stable area. Therefore, the relationship between the signal generated by controller (ui) and tire slip can be considered linear according to Eq. (24).

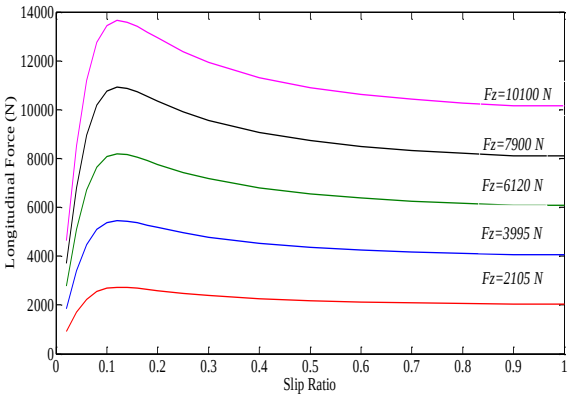

Fig. 2. Longitudinal force curves of a tire versus wheel slip ratio for different normal forces on a road with unit adhesion coefficient

$$\frac{s_i F_{zi}}{u_i F_{zav}} = \zeta_i \tag{24}$$

In Eq. (24), F_{zav} is the wheels average normal force used for equation normalization and ζ_i is the linearized curve slope, which is almost the same for intact motors assuming similar adhesion coefficient between the tire

and the road. However, in case of fault and reduction of faulty motor gain, the faulty motor torque is reduced; and thus, the controller significantly increases controlling signal for existing motors on the faulty side of the vehicle to maintain vehicle stability.

The generated torque and slip consistently increase by enlarged control signal in intact motor; however, it is less for faulty motor due to reduced gain; therefore, the slip will be lower than the expected amount. As a result, ζi is less for faulty wheel. Also, for the conditions that the fault is an increased malfunction type, ζi will be high. Therefore, the fault detection signal (res) can be defined as Eq. (25).

$$\begin{cases} res = \left\| \Delta_l \right| - \left| \Delta_r \right\| \\ \Delta_l = \zeta_{fl} - \zeta_{rl} \\ \Delta_r = \zeta_{fr} - \zeta_{rr} \end{cases} \quad (25)$$

According to Eq. (26), if all the motors of vehicle are intact, the *res* value would be small and close to zero; but, by the fault occurrences, the amount of *res* will increase. Hence, comparing the *res* with a threshold value (ε) that can be determined through considering the uncertainties in model and parameters through trial and error, the fault is detected. To determine this threshold, an artificial neural network can be trained by using the intact vehicle information. In this paper, assuming the 5% acceptable fault due the uncertainties, a neural network has been trained for obtaining ε. Neural network inputs include steering wheel angle, vehicle speed, vehicle yaw rate, longitudinal slip ratio of the four wheels, and the motors' control signals. The output is a threshold signal.

$$\begin{cases} res > \varepsilon \rightarrow with\ fault \\ res \le \varepsilon \rightarrow\ no\ fault \end{cases} \quad (26)$$

The fault will be on side of the vehicle where has greater Δ.

$$\begin{cases} \left| \Delta_l \right| > \left| \Delta_r \right| \rightarrow fault\ in\ left\ side \\ \left| \Delta_l \right| < \left| \Delta_r \right| \rightarrow fault\ in\ right\ side \end{cases} \quad (27)$$

In case of decreasing fault in the faulty side of the vehicle, the faulty wheel will have a smaller gain size ζ_i and in case of the additive fault, ζ_i will be larger. In Eq. (28), ζ_f is for the faulty motor and ζ_h for the intact motor.

$$\begin{cases} \text{Decreasing Fault: } \left| \zeta_f \right| < \left| \zeta_h \right| \\ \text{Additive Fault: } \left| \zeta_f \right| > \left| \zeta_h \right| \end{cases} \quad (28)$$

In general, fault type and location are illustrated in flow chart in Fig. 3.

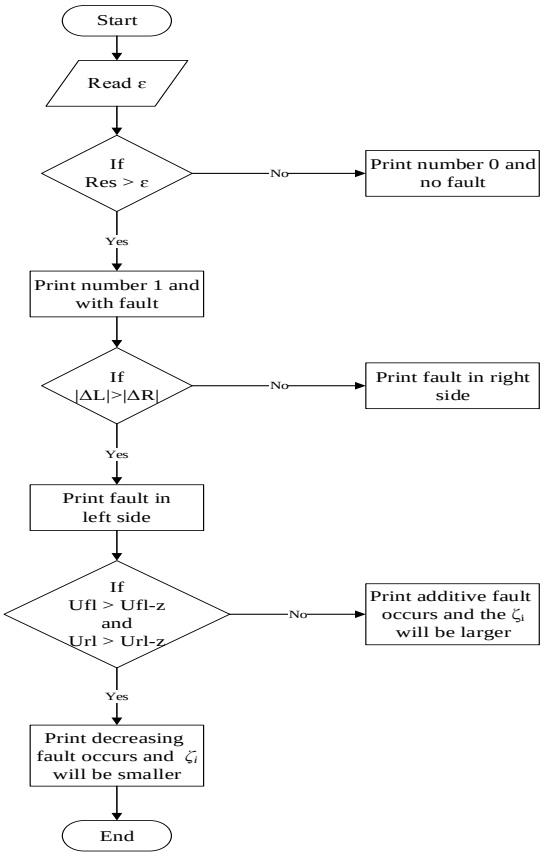

Fig. 3. Fault identification and isolation system flowchart

To modify the controller, it requires estimating the faulty motor controlling gain. To obtain the approximate value of this gain, the simplified dynamics equation of the wheel and the motor can be used according to Eq. (29) [18]. In the following equation, *I* represents the wheel moment of inertia.

$$I\dot{\omega}_i = -R_{eff} F_{xi} + k_i u_i \quad (29)$$

4.2. Controller modification

In addition to detect fault location and its value, the use of faulty motor should be limited, too. Turning off the faulty motor may be a solution; however, it leads to the loss of much of traction force and reduction of vehicle ability meeting driver's request. So, in this paper, it is suggested to reduce the amount of pressure on faulty motor in accordance with the fault occurred avoiding the vehicle potential loss, the faulty motor is immune from further damage. Thus, to calculate motors' control signal at the faulty side of the vehicle, the following cost function is recommended.

$$\begin{cases} J = w_h u_h^2 + w_f u_f^2 \\ k_h F_{zh} u_h + k_f F_{zf} u_f = \Omega \end{cases} \quad (30)$$

In the above equation, u_h and u_f are control signals of the intact and faulty motors, respectively; kh and k_f are controlling gains of the intact and faulty motor; Fzh and

F_{zf} are the normal forces of the intact and faulty wheels, respectively; and, w_h and w_f are weighting coefficients and Ω is a constant amount. Assuming $w_f = w_h k_h / k_f$, the optimal response to the cost function (J) is as Eq. (31).

$$\frac{u_h}{u_f} = \frac{F_{zh} k_h^2}{F_{zf} k_f^2} = \Psi \tag{31}$$

Replacing Ψ with D_1 and D_2 in Eqs. (22) and (23), the controller can be modified. The system control block diagram is represented in Fig. 4.

5. SIMULATION RESULTS

The proposed controller is simulated on a four-wheel drive electric vehicle without differential in C-Class using MATLAB and CARSIM softwares. The parameters of the assumed vehicle are provided in Table 2. The performance of the vehicle has been simulated with the sinusoidal steering maneuver and double lane change quick start (DLCQS) maneuver during acceleration. Also, the performance of the fault detection system and the controller with a faulty traction motor, have been simulated in a straight line and with sinusoidal maneuver.

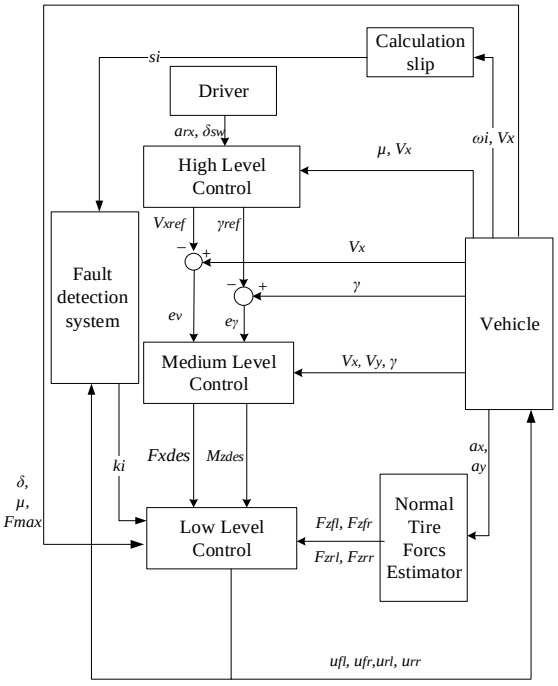

Fig. 4. Block diagram of closed-loop control system

5.1. Testing vehicle stability through steering maneuver

At the first test, the vehicle accelerates from 10 m/s to 30 m/s within 20 seconds and the driver simultaneously changes the steering wheel angle with a range of 25 degrees in a sinusoidal way. The road surface friction coefficient with the tire is 0.85. At the 5th second, a motor fault occurs in the front-left motor that causes the gain of the motor to reduce from 1 to 0.5. The control gain of the other in-wheel motors are maintained at 1.

Table 2. Parameters of the vehicle model

	Notation	Unit	Value
Vehicle total mass	M	kg	1554
Vehicle sprung mass	m	kg	1270
Wheel total mass	m_w	kg	71
Tire effective radius	R_{ef}	m	0.308
Half of Lateral distance between centers of tire	l_s	m	0.77
Distance from the front axle to the mass center	l_f	m	1.016
Distance from the rear axle to the mass center	l_r	m	1.564
Aerodynamic drag coefficient	C_d	-	0.3
Yaw inertia of the vehicle	I_z	$kg.m^3$	1536.7

Vehicle behavior is simulated by controlling rate and without yaw rate control (only with speed control). Furthermore, the proposed controller performance is compared with the controller used in [14, 16].This compared controller has been designed based on Lyapunov function theorem. Assume two in-wheel motors in the left side of the vehicle have similar effect on the yaw dynamics, and similarly, the effects of both motors in the right side are the same. Consequently, the control signals for driving the in-wheel motors can be expressed as Eq. (32) [16].

$$\begin{cases} u_l = \dfrac{R_{eff}\left(M k_{rz}\left(L_1 \dot{e}_v + \dot{v}_{xref} - f_1(X)\right) - \dfrac{I_z}{l_s} k_{rx}\left(L_2 \dot{e}_\gamma + \dot{\gamma}_{ref} - f_3(X)\right)\right)}{k_{lx} k_{rz} + k_{rx} k_{lz}} \\ u_r = \dfrac{R_{eff}\left(M k_{lz}\left(L_1 \dot{e}_v + \dot{v}_{xref} - f_1(X)\right) + \dfrac{I_z}{l_s} k_{lx}\left(L_2 \dot{e}_\gamma + \dot{\gamma}_{ref} - f_3(X)\right)\right)}{k_{lx} k_{rz} + k_{rx} k_{lz}} \end{cases} \tag{32}$$

Where, u_l and u_r are the control signals for the rear-left and rear-right motors, respectively. Therefore, the control signals for the front-left and right motors are as $\lambda_l u_l$ and $\lambda_r u_r$, respectively. However, λ_r and λ_l can be chosen as one because of the similar effects of the motors in one side of the vehicle. L_1 and L_2 are the constant coefficients, and k_{lx}, k_{rz}, k_{rx}, and k_{lz} are defined as Eq. (33) [16].

The vehicle's speed curves for all three simulated controllers are represented in Fig. 5. Also, the vehicle speed curves are zoomed from 4.95s to 5.1s in Fig. 5.

$$\begin{cases} k_{lx}=k_{fl}\cos\delta+k_{rl} \\ k_{rx}=k_{fr}\cos\delta+k_{rr} \\ k_{lz}=k_{fl}\cos\delta+k_{rl}-k_{fl}\dfrac{l_f\sin\delta}{l_s} \\ k_{rz}=k_{fr}\cos\delta+k_{rr}+k_{fr}\dfrac{l_f\sin\delta}{l_s} \end{cases} \quad (33)$$

The simulated vehicle yaw rate curves using the three controllers are shown in Fig. 6. Also, yaw rate curves are zoomed from 4.5s to 6.5s in Fig. 6. The results indicate that using the proposed controller, the vehicle becomes more stable and tracking the speed reference and yaw rate reference are sufficiently accurate. As a result, in addition to maintaining the stability of the vehicle, the driver's requests are also satisfied. Figs. 5 and 6, illustrate the proposed controller has the better speed and yaw rate tracking than the compared controller, especially when there is a fault in one of actuators. Figs. 7 and 8, illustrates the control signal applied to the electric drive (reference torques) with proposed controller and the compared controller, respectively. At *t*=5s, the controllers enhance the control effort on the faulty side of the vehicle to overcome the faults effects on the vehicle performances.

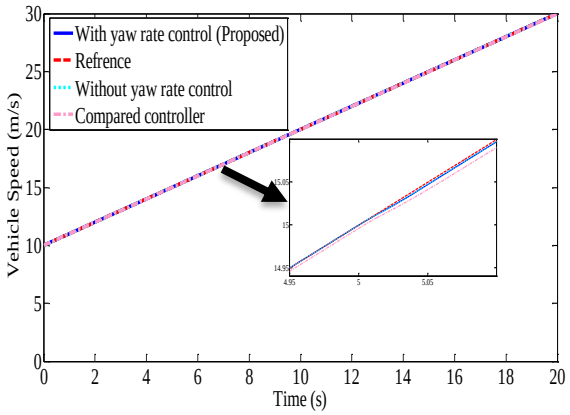

Fig. 5. Vehicle speed curves in the sinusoidal steering change with a fault in the front-left motor at t=5s

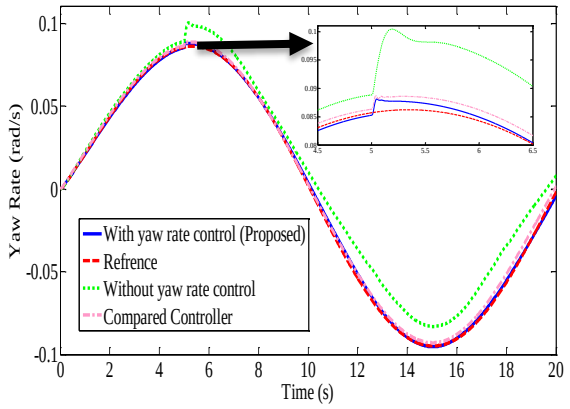

Fig. 6. Vehicle yaw rate curves in the sinusoidal steering change with a fault in the front-left motor at t=5s

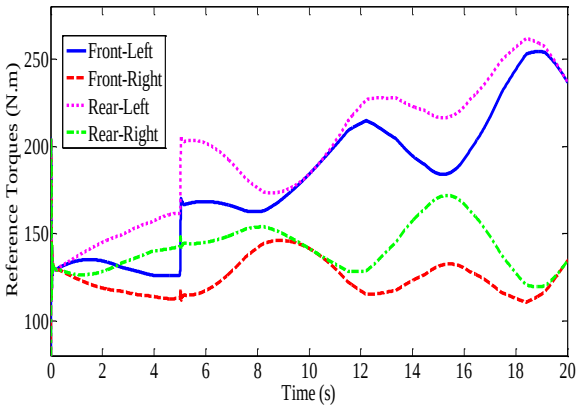

Fig. 7. Torque references for the electric motors with the proposed controller

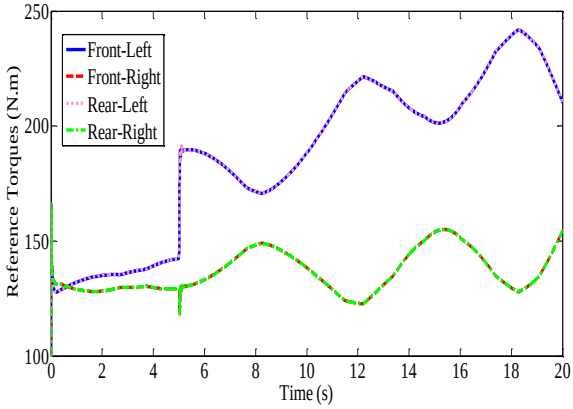

Fig. 8. Torque references for the electric motors with the compared controller

The proposed and compared controllers are simulated in the standard CARSIM double lane change quick start (DLCQS) maneuver. This test is done for showing the vehicle performance in the severer steering condition and analyzing the controllers' accuracy. The vehicle is accelerated from 10m/s to 30m/s in 20s on the road with 0.85 friction coefficient and there is not any actuator fault considered. Figures 9 and 10 illustrate the vehicle can accurately track the reference speed and yaw rate in this maneuver, respectively.

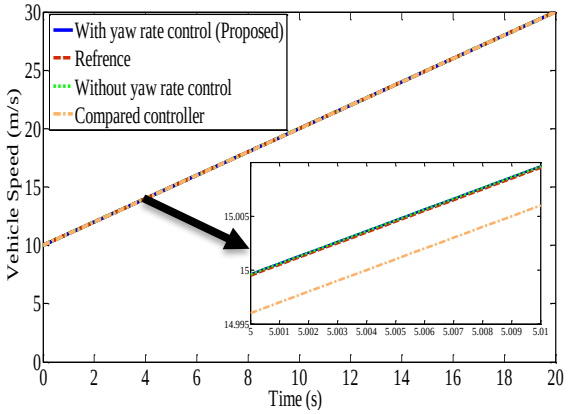

Fig. 9. Vehicle speed curves on the DLCQS maneuver

Also, the vehicle speed curves for different controllers are zoomed from 5s to 5.01s in Fig. 9, and the vehicle yaw rate curves are zoomed from 7s to 8s in Fig. 11. In this paper, mean square error (MSE) is utilized as Eq. (34) to performance assessment of the controllers [33].

$$MSE = \frac{1}{N}\sum_{i=1}^{N} e_v(i)^2 + \frac{1}{N}\sum_{t=1}^{N} e_\gamma(i)^2 \qquad (34)$$

In Eq. (34), N is the number of samples, $e_v(i)$ and $e_\gamma(i)$ are the error of speed and yaw rate in i-th sample, respectively. The calculated MSEs for the simulated controllers on the DLCQS maneuver have been included in Table 3. As visible from Table 3, the proposed controller has the lowest MSE. Consequently, the proposed controller is the most accurate among the compared controllers.

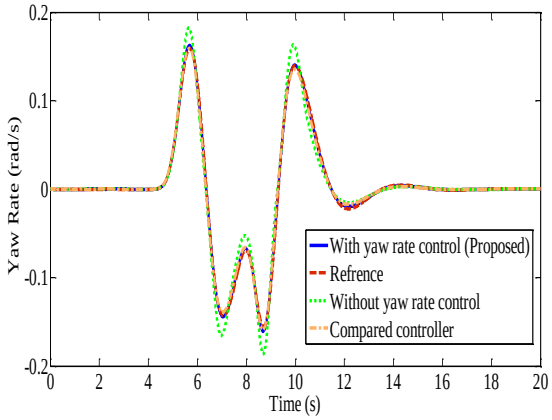

Fig. 10. Vehicle yaw rate curves on the DLCQS maneuver

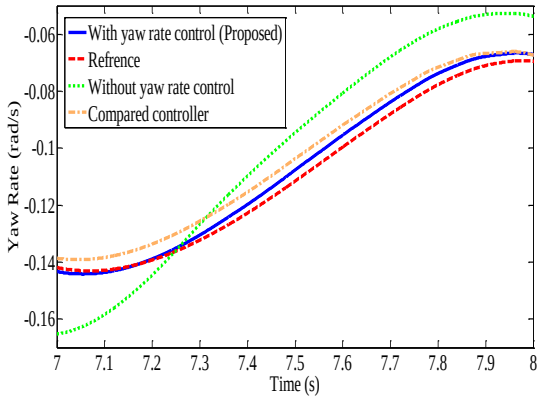

Fig. 11. Zoomed vehicle yaw rate curves on the DLCQS maneuver from 7s to 8s

5.2. Controller performance in case of fault occurrence

Suppose that the given vehicle is moving at the speed of 50 km per hour in a straight line on a road with a friction coefficient of 0.85. At the 5th second, a fault occurs in the front-left motor leading to reduction in motor control gain up to 0.8 of the initial value; as the sliding mode control used in the proposed controlling structure and the controller great robustness against disturbance and uncertainty in model parameters [13, 30], it is expected that the vehicle could tolerate the faulty condition.

Table 3. Mean square errors

	Yaw Rate MSE ($\times 10^{-5}$)	Speed MSE ($\times 10^{-5}$)	Total MSE ($\times 10^{-5}$)
Proposed Controller	0.3746	0.0093	0.3839
Compared Controller	1.282	2.8972	4.1792
Without Yaw Control	9.5056	0.0103	9.5159

In addition, once fault occurred, the fault identification system shows fast response, identifies fault location, estimates fault value, and modifies the controller.

The neural network output signal is used as the threshold signal (ε) for comparing with the res signal. With regard to the acceptability of 5% malfunction for considering the uncertainties, the data from the vehicle with a 5% fault is used for tuning the nueral network. In Fig. 12, at the moment of 5 seconds, a fault occurs in the left-front motor and leads to gain of 0.8 of the intial amount. Thus, according to Fig. 12, it can be observed that the fault was more than the acceptable amount. Therefore, the residual signal (res) produced a value larger than ε and the fault is detected. Fig. 13 shows Δr and Δl in driving on a the straight line. It can be seen that after 5 seconds, Δl increases in comparison to Δr, which indicates a fault in the vehicle left side.

Figure 14, presents ξi curve for four wheels in driving on a straight line. It can be seen that after 5 seconds, the faulty wheel (left front) has smaller ξ than the heath wheels on the left and right of the vehicle. Fig. 15, also shows the wheels' torque curves a fault at the moment of 5 seconds.

In another test, the given vehicle moves at 60 km/h in a sinusoidal steering maneuver with a range of 20 degrees on a road with a friction coefficient of 0.85. At the moment 5 seconds, a fault occurs in the front left motor leading to the loss of motor gain, in this motor up to 0.8 of the initial amount, which is considered acceptable according to previous test for an accuracy of about 5%. According to Fig. 16, residual signal (res) and the threshold value are derived from neural network in the sinusoidal steering maneuver. It can be seen that at the time of 5 seconds, a fault occurs in one of the actuators and the fault is detected. Fig. 17 illustrates Δr and Δl curves in the sinusoidal steering maneuver.

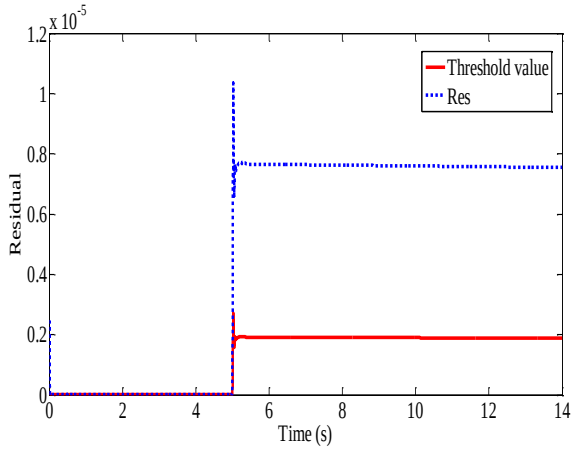

Fig. 12. Residual signal curve and threshold amount in driving on a straight line

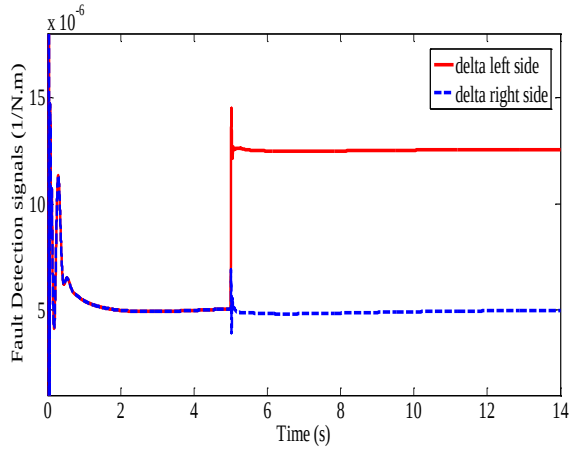

Fig. 13. Δ_r and Δ_l signals with the fault occurring at the time of 5 seconds in the front left motor in the straight line

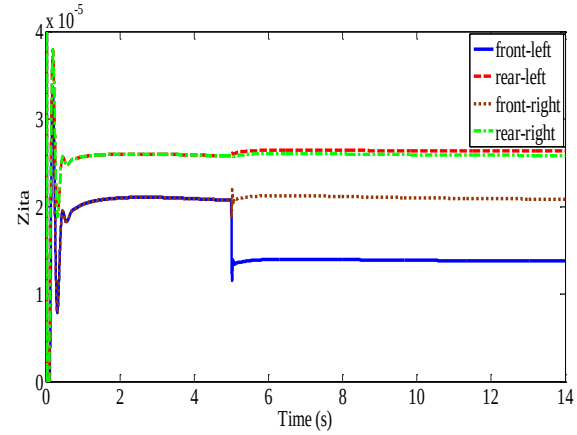

Fig. 14. ξ_i for four wheels in driving on a straight line

It can be observed that Δl increases after 5 seconds in comparison to Δr indicating that there is a fault in the left side of the vehicle. Fig. 18, shows ξi curve for four wheels in the sinusoidal steering maneuver; it is observed that after 5 seconds, the faulty wheel (left front) has a ξ smaller than normal wheels on the left and right of the vehicle. Fig. 19, also indicates the torque applied on the four driving wheels with a fault at 5 seconds in sinusoidal steering maneuver.

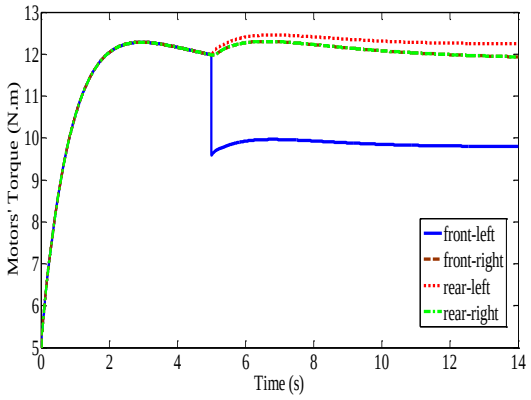

Fig. 15. The wheels torque with a fault at 5 seconds when driving on a straight line

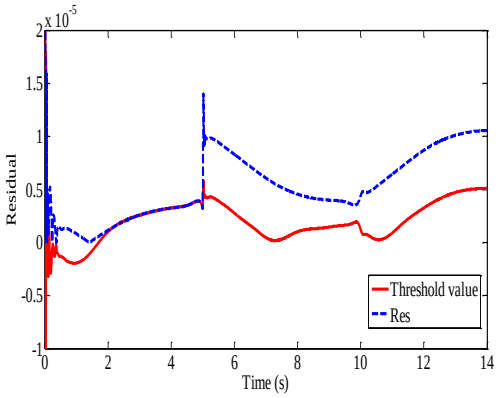

Fig. 16. Residual signal curve and threshold amount with a fault occurring at the time of 5 seconds in sinusoidal steering maneuver

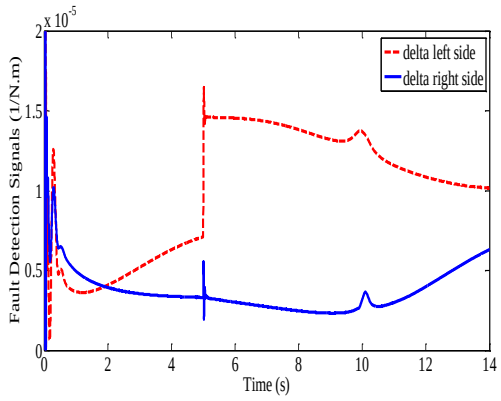

Fig. 17. Δ_r and Δ_l signals with a fault occurring at the time of 5 seconds in the front left motor in sinusoidal steering maneuver

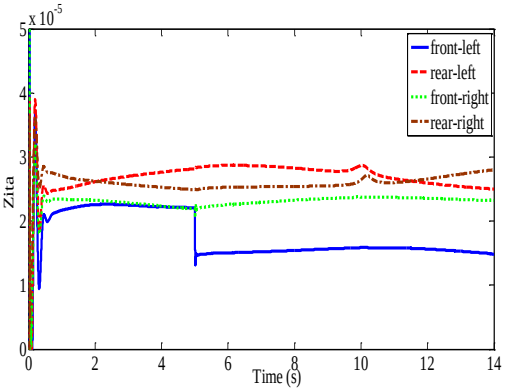

Fig. 18. ξ_i for four wheels in sinusoidal steering maneuver

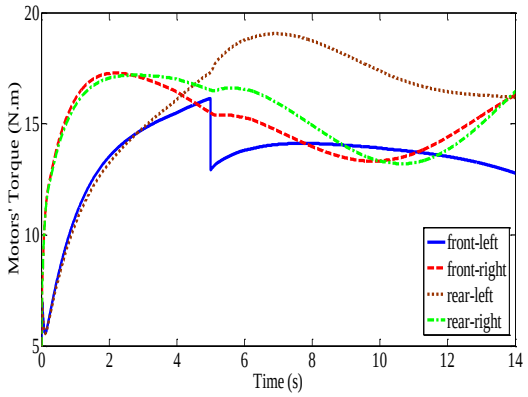

Fig. 19. The torque applied on the wheels with the fault at the time of 5 seconds in sinusoidal steering maneuver

6. CONCLUSION

In this paper, a three-layer controller using the sliding mode control for lateral stability of the four wheel independent drive electric vehicles and an entirely new method of fault identification and isolation have been suggested. The proposed performance of control system has been verified through simulation on MATLAB and CARSIM environments. The simulation results indicate the high accuracy of the controller to track the longitudinal speed reference and yaw rate reference. According to simulation results, the proposed fault detection system is highly accurate and fault location is quickly detected. Then, the controller is modified according to new controller gain of the electric motor after the fault. Consequently, less damage is exerted on the faulty traction motor. The proposed controller is simple and accurate for practical use in the vehicle.

REFERENCES

[1] J. Santiago, H. Bernhoff, B. Ekergård, S. Eriksson, S. Ferhatovic, R. Waters, and M. Leijon, "Electrical motor drivelines in commercial all-Electric vehicles: A review," *IEEE Trans. Veh. Technol.*, vol. 61, no. 2, pp. 475-484, 2012.

[2] A. Badri and K. Hoseinpour Lonbar, "Stochastic multiperiod decision making framework of an electricity retailer considering aggregated optimal charging and discharging of electric vehicles," *J. Oper. Autom. Power Eng.* , vol. 3, no. 1, pp. 34-46, 2015.

[3] M. Shino and M. Nagai, "Independent wheel torque control of small-scale electric vehicle for handling and stability improvement," *JSAE Rev.*, vol. 24, no. 4, pp. 449-456, 2003.

[4] R. Wang and J. Wang, "Fault tolerant control for electric ground vehicles with independently actuated in-wheel motors," *ASME J. Dyn. Syst. Meas. Contr.*, vol. 134, no.2, pp. 1-10, 2012.

[5] W. Liang, H. Yu, R. McGee, M. Kuang, and J. Medanic, "Vehicle pure yaw moment control using differential tire slip," *Am. Contr. Conf.*, pp. 3331-3336, 2009.

[6] F.Tahami, R. Kazemi, and S. Farhanghi, "A novel driver assist stability system for all-wheel electric vehicles," *IEEE Trans. Veh. Technol.*, vol. 52, no. 3, pp. 683-692, 2003.

[7] F. Tahami, S. Farhanghi, and R. Kazemi, "A fuzzy logic direct yaw-moment control system for all-wheel drive electric vehicles," *Veh. Syst. Dyn.*, vol. 41, no. 3, pp. 203-221, 2004.

[8] F. Tahami, S. Farhanghi, R. Kazemi, and B. Samadi, "Fuzzy based stability enhancement system for a four motor electric vehicle," *J. Passengers Cars Mech. Syst.*, pp.1825-1833, 2002.

[9] F. Tahami, S. Farhanghi, R. Kazemi, "Direct yaw control of an all-wheel-drive ev based on fuzzy logic and neural networks," *Proc. SAE World Congr.*, paper no.2003-01-0956, 2003, pp. 1-9.

[10] A. Goodarzi and E. Esmailzadeh, "Design of a VDC system for all-wheel independent drive vehicles," *IEEE Trans. Mechatron.*, vol. 12, no. 6, pp. 632-639, 2007.

[11] C. Geng, L. Mostafai, M. Denai, and Y. Hori, "Direct yaw-moment control of an in-wheel-motored electric vehicle based on body slip angle fuzzy observer," *IEEE Trans. Ind. Electron.*, vol. 56, no. 5, pp. 1411-1419, 2009.

[12] D. Kim, S. Hwang, and H. Kim, "Vehicle stability enhancement of four-wheel-drive hybrid electric vehicle using rear motor control," *IEEE Trans. Veh. Technol.*, vol. 57, no. 2, pp. 727-735, 2008.

[13] H. Alipour, M. B. Bana Sharifian, and M. Sabahi, "A modified integral sliding mode control to lateral stabilisation of 4-wheel independent drive electric vehicles," *Veh. Syst. Dyn.*, vol. 52, no.12, pp.1584-1606, 2014.

[14] H. Alipour, M. Sabahi, and M. B. Bana Sharifian, "Lateral stabilization of a four wheel independent drive electric vehicle on slippery roads," *Mechatron.*, vol.30, no. 1, pp. 275-285, 2014.

[15] H. Yang, V. Cocquempot, and B. Jiang, "Optimal fault-tolerant path-tracking control for 4ws4wd electric vehicles," *IEEE Trans. Intell. Transp. Syst.*, vol. 11, no. 1, pp. 237- 243, 2010.

[16] R. Wang and J. Wang, "Fault-tolerant control with active fault diagnosis for four-wheel independently driven electric ground vehicles," *IEEE Trans. Veh. Technol.*, vol. 60, no. 9, pp. 4276-4287, 2011.

[17] R. Wang and J. Wang, "Passive actuator fault-tolerant control for a class of overactuated nonlinear systems and applications to electric vehicles," *IEEE Trans. Veh. Technol.*, vol. 62, no. 3, pp. 972-985, 2013.

[18] R. Wang and J. Wang, "Actuator-redundancy-based fault diagnosis for four-wheel independently actuated electric vehicles," *IEEE Trans. Intell. Transp. Syst.*, vol. 14, no. 1, pp. 239-249, 2014.

[19] M. A. Djeziri, R. Merzouki, B. O. Bouamama, and M. Ouladsine, "Fault diagnosis and fault-tolerant control of an electric vehicle over actuated," *IEEE Trans. Veh. Technol.*, vol. 62, no. 3, pp. 986-994, 2013.

[20] R. Loureiro, S. Benmoussa, Y. Touati, R. Merzouki, and B. O. Bouamama, "Integration of fault diagnosis and fault-tolerant control for health monitoring of a class of MIMO intelligent autonomous vehicles," *IEEE Trans. Veh. Technol.*, vol. 63, no. 1, pp. 30-39, 2014.

[21] Y. L. Murphy and M. Abul Masrur, "Model-based fault diagnosis in electric drives using machine learning," *IEEE/ASAME Trans. Mechatron.*, vol. 11, no. 3, pp. 290-303, 2006.

[22] M. Moazen, and M. Sabahi, "Electric differential for an electric vehicle with four independent driven motors and four wheels steering ability using improved fictitious

master synchronization strategy," *J. Oper. Autom. Power Eng.*, vol. 2, no. 2, pp. 141-150, 2014.

[23] F. J. Perez-Pinal, I. Cervantes, and A. Emadi, "Stability of an electric differential for traction applications," *IEEE Trans. Veh. Technol.*, vol. 58, no. 7, pp. 3224-3233, 2009.

[24] B. Li, A. Goodarzi, A. Khajepour, S.-k. Chen, and B. Litkouhi, "An optimal torque distribution control strategy for four-independent wheel drive electric vehicles," *Veh. Syst. Dyn.*, vol. 53, no. 8, pp. 1172-1189, 2015.

[25] L. De Novellis, A. Sorniotti, P. Gruber, J. Orus, J.-M. R. Fortun, J. Theunissen, and J. De Smet, "Direct yaw moment control actuated through electric drivetrains and friction brakes: Theoretical design and experimental assessment," *Mechatron.*, vol. 26, pp. 1-15, 2015.

[26] B. Li, H. Du, and W. Li, "Fault-tolerant control of electric vehicles with in-wheel motors using actuator-grouping sliding mode controllers," *Mech. Syst. Signal Process.*, vol. 72, no.1, pp. 462-485, 2016.

[27] L. Zhai, T. Sun, and J. Wang, "Electronic stability control based on motor driving and braking torque distribution for a four in-wheel motor drive electric vehicle," *IEEE Trans. Veh. Technol.*, vol. 65, no. 6, pp. 4726-4739, 2016.

[28] R. Rajamani, *Vehicle Dynamics and Control*," 2nd Ed. New York: *Springer*, 2012.

[29] J. A. Cabrera, A. Ortiz, E. Carabias, and A. Simon, "An alternative method to determine the magic tire model parameters using genetic algorithms," *Veh. Syst. Dyn.*, vol. 41, no. 2, pp. 109-127, 2014.

[30] H. Alipour, M. B. Bannae Sharifian, and H. Afsharirad, "A PID sliding mode control for ropeless elevator maglev guiding system," *Energy Power Eng.*, vol. 4, no. 3, pp. 158-164, 2012.

[31] M. J. Kharaajoo and F. Besharati, "Sliding mode traction control of an electric vehicle with four separate wheel drives," *Proc. IEEE Int. Conf. Emerging Technol. Factory Autom.*, vol.2, 2003, pp. 29-296.

[32] N. Mutoh, "Driving and braking torque distribution methods for front-and rear-wheel-independent drive-type electric vehicles on roads with low friction coefficient," *IEEE Trans. Ind. Electron.*, vol. 59, no. 10, pp. 3919-3933, 2012.

[33] E. L. Lehmann and G. Casella, "*Theory of Point Estimation*," 2nd Ed, *Springer*, 2006.